Hindawi Publishing Corporation
Advances in Physical Chemistry
Volume 2012, Article ID 236750, 12 pages
doi:10.1155/2012/236750

Research Article

New *ab Initio* Potential Energy Surfaces for the Renner-Teller Coupled $1^1A'$ and $1^1A''$ States of CH_2

Haitao Ma,[1] Chunfang Zhang,[1] Zhijun Zhang,[1] Xiaojun Liu,[2] and Wensheng Bian[1]

[1] *Beijing National Laboratory for Molecular Sciences, Institute of Chemistry, Chinese Academy of Sciences, Beijing 100190, China*
[2] *Key Laboratory of Luminescence and Optical Information, Ministry of Education, Institute of Optoelectronic Technology, Beijing Jiaotong University, Beijing 100044, China*

Correspondence should be addressed to Wensheng Bian, bian@iccas.ac.cn

Received 31 August 2011; Revised 31 October 2011; Accepted 9 November 2011

Academic Editor: António Varandas

New *ab initio* potential energy surfaces (PESs) for the two lowest-lying singlet $1^1A'$ and $1^1A''$ electronic states of CH_2, coupled by the Renner-Teller (RT) effect and meant for the spectroscopic study, are presented. The surfaces are constructed using a dual-level strategy. The internally contracted multireference configuration interaction calculations with the Davidson correction, using the *aug-cc-pVQZ* basis set, are employed to obtain 3042 points at the lower level. The core and core-valence correlation effects are taken into account in the *ab initio* calculations with a modified optimized *aug-cc-pCVQZ* basis set for the higher-level points. The analytical representations of these PESs, with the inclusion of the nonadiabatic RT terms, are obtained by the nonlinear least-squares fit of the calculated points to three-body expansion. Quantum dynamical calculations are performed on these PESs, and the computed vibronic energy levels for the two singlet electronic states are in excellent agreement with experiment.

1. Introduction

The CH_2 biradical has been the subject of many theoretical and experimental studies, due to its distinct electronic characteristics and chemical and physical properties. It is the direct chemical precursor of the widely observed CH radical [1]. As a crucial link in the photodissociation sequence of cometary methane, CH_2 plays a significant role in the chemistry of hydrocarbon combustion and the astrophysics of interstellar medium [2–5].

Since Herzberg and Johns [2] carried out a detailed analysis of the high-resolution absorption spectrum of the singlet CH_2 in the near ultraviolet region half a century ago, several groups [6–11] have observed the direct absorption spectra or subsequent monitoring of fluorescence via laser-induced fluorescence, stimulated emission pumping, dispersed fluorescence, and so forth. Experimental investigations of the spectroscopy provided abundant and precise rovibronic energy levels [12–16]. Recently, bands in the CH_2 $\tilde{b}^1B_1$-$\tilde{a}^1A_1$ transition between 12500 and 13000 cm^{-1} were recorded at Doppler-limited resolution utilizing a transient frequency-modulation (FM) laser absorption spectrometer by Chang and coworkers [16]. An unexpected and particularly complicated rovibronic structure was detected for $b(1,1,0)^1$ and $b(0,3,0)^1$ vibronic levels. Comparison of the calculated spectra on the available potential energy surfaces (PESs) [17–19] with the experimental spectra of Herzberg and Johns [2] indicates that the labeling of some vibrational levels is quite inconsistent, which can be ascribed to the local perturbations from the vibrational resonances and Renner-Teller (RT) effect.

The study of the RT effect on the vibronic levels for nonlinear three-atom molecules has been an active area for several decades [8, 17, 20–24]. The $\tilde{b}^1B_1$-$\tilde{a}^1A_1$ transition of CH_2, which is seen in the red and yellow parts of the spectrum, is one of the best examples in which the RT coupling should be observed [5]. One of the consequences of the RT coupling is the inversion of the K_a rotational structure in the lower component state ($\tilde{a}^1A_1$) near the barrier to linearity. As explained by Jungen et al. [25], this reordering

of the K_a energy levels results from the transformation at high bending levels from bent to linear configurations [8]. The two lowest-lying singlet electronic states of CH_2, which become a degenerate Δ pair at linearity, interact strongly with each other and are coupled dynamically [17, 24].

Theoretically, some researchers [3, 4, 26] examined a few electronic states of CH_2 with state-of-the-art *ab initio* methods and provided significant clues to the understanding of the electronic structures. Bussery-Honvault and coworkers [27] computed an *ab initio* global PES for the first singlet state of CH_2, where a mixed numerical and analytical method was employed in the PES construction. This surface shows no barrier for the C_{2V} insertion, while a barrier of 4319 cm^{-1} (12.35 kcal/mol) is present for the collinear approach. Unfortunately, visible discrepancies were found between the theoretical calculations on this surface and the experimental results [28]. Later, using the same *ab initio* methodology and similar fitting process, Bussery-Honvault and coworkers [29] constructed a PES for the second singlet state of CH_2; it should be mentioned that their two lowest-lying singlet PESs are not degenerate at linearity. Joseph and Varandas [30] constructed a more accurate PES for the lowest singlet state of CH_2 with the DMBE scaled-external-correlations method [31] and obtained very good agreement with the experimental rate constants, which recommends it for future dynamics studies [30, 32]. Furthermore, Dawes et al. [33] constructed the lowest singlet PES using the local interpolative moving least squares method and performed further spectroscopic calculations, which yielded $J = 0$ vibrational frequencies with a root-mean-square error of a few wavenumbers relative to available measurements.

Liu and co-workers [34] revealed various PES intersection seams among the $1^1A'$, $2^1A'$, $3^1A'$, $1^1A''$ and $2^1A''$, states in the $C(^1D)H_2$ reactive system systematically and determined the minimum energy crossing points (MECPs) accurately. The nonadiabatic interaction near MECPs may play an important role in spectroscopy and dynamics [35–40]. The lowest MECP [34] in $C(^1D)H_2$, which is only 8797 cm^{-1} above the CH_2 $1^1A'$ minimum and much lower in energy than all the other MECPs, is between the two low-lying $\widetilde{a}^1A_1$ and $\widetilde{b}^1B_1$ states, which become the degenerate Δ_g pair at linearity and hence are strongly coupled by the RT effect. All the other MECPs [34] are above or somewhat below the $C(^1D)+H_2$ asymptote in energy and thus are not expected to intervene most of the vibronic spectra of the two lowest-lying singlet electronic states. However, it is clear that the RT coupling must be taken into account in the vibronic energy level calculations of the two lowest-lying states.

A few PESs for the RT coupled $\widetilde{a}^1A_1$ and $\widetilde{b}^1B_1$ states have been developed to simulate the vibronic structure and electronic spectrum with the vibronic coupling included [17, 19, 24, 41]. However, the *ab initio* PESs of Green Jr. et al. [17] were empirically adjusted or shifted to fit the experimental data; other PESs [19, 24, 41] were constructed by fitting experimental data and a few *ab initio* points [13]. However, there are therefore accurate and fully *ab initio* PESs for the two lowest-lying singlet electronic states $1^1A'$ and $1^1A''$ of CH_2 with the RT terms required.

So far most of the *ab initio* work concerning CH_2 has been based on the traditional correlated *ab initio* electronic structure calculations, that is, the so-called frozen core approximation, in which correlation effects involving the electrons in *1s* core orbital of carbon are neglected. However, as noted by Peterson and Dunning [42], if the goals of a calculation are to obtain chemical accuracy of thermochemical properties, the effects of correlating the electrons in the core orbital generally must be addressed in the calculations. Of course, *ab initio* calculations including correlation effects of core electrons are very time-consuming. In this work, not only appropriate active space but also an optimized basis set with additional functions for describing core and core-valence correlation effects (called CV) is employed in our *ab initio* calculations, which can also guarantee that the two lowest-lying singlet PESs are degenerate at linearity. We further construct fully *ab initio* PESs for the two lowest-lying singlet electronic states $1^1A'$ and $1^1A''$ of CH_2 with the inclusion of the nonadiabatic RT terms.

The organization of the present article is as follows. Section 2 describes the *ab initio* electronic structure calculations. The fitting of the *ab initio* energy points is presented in Section 3. The fitted PESs of CH_2 (called MZB) and vibronic energy level calculations are discussed in Section 4. Finally, a summary is given in Section 5.

2. Electronic Structure and *ab Initio* Calculations

2.1. Electronic Structure. For computational convenience, the molecule is placed in the *yz* plane, and the electronic configuration of ground state is $(1a_1)^{\uparrow\downarrow}(2a_1)^{\uparrow\downarrow}(1b_2)^{\uparrow\downarrow}(3a_1)^{\uparrow}(1b_1)^{\uparrow}$. The $(1a_1)$ and $(2a_1)$ molecular orbitals (MOs) mostly have carbon *1s* and *2s* characters, respectively. The $(3a_1)$, $(1b_1)$, and $(1b_2)$ MOs mainly have the carbon *2p* character lying along the twofold *z* axis, perpendicular and parallel with respect to the *yz* plane, respectively. In the C_s symmetry, the a_1 and b_2 orbitals become the a' orbitals, and the b_1 and a_2 orbitals become the a'' orbitals.

The electronic configurations of CH_2 can be represented as shown in Table 1 in the C_{2V} or C_s symmetry.

The $\widetilde{X}^3B_1$ and $\widetilde{b}^1B_1$ states, which share the same spatial orbital configuration with two open-shell electrons parallelly or antiparallelly distributed in the outer $3a_1$ and $1b_1$ orbitals, correspond to the triplet and singlet configurations, respectively. While the $\widetilde{a}^1A_1$ and $\widetilde{c}^1A_1$ states correspond primarily to configurations with double occupation of the $3a_1$ or $1b_1$ orbital, they could be appropriately described by the two main configuration wave functions. The two CI coefficients C_1 and C_2 for $\widetilde{a}^1A_1$ have opposite signs with $|C_1| \geq |C_2|$, while those for the $\widetilde{c}^1A_1$ state have the same sign with $|C_3| \leq |C_4|$. Hence, multireference methods are required for an accurate *ab initio* description of the above excited states. The $\widetilde{a}^1A_1$ and $\widetilde{b}^1B_1$ states become the degenerate $1^1\Delta_g$ pair at linearity and hence are strongly mixed by the RT coupling, which is important to the vibronic calculations. The $\widetilde{c}^1A_1$ state correlates with the $1^1\Sigma_g^+$ state at linearity. The next two states, 1^1A_2 and 1^1B_2, become the degenerate $1^1\Pi_u$ pair

Table 1

$\widetilde{X}^3B_1$:$(1a_1)^{\uparrow\downarrow}(2a_1)^{\uparrow\downarrow}(1b_2)^{\uparrow\downarrow}(3a_1)^{\uparrow}(1b_1)^{\uparrow}$	X^3A'':$(1a')^{\uparrow\downarrow}(2a')^{\uparrow\downarrow}(3a')^{\uparrow\downarrow}(4a')^{\uparrow}(1a'')^{\uparrow}$
$\widetilde{a}^1A_1$:$C_1(1a_1)^{\uparrow\downarrow}(2a_1)^{\uparrow\downarrow}(1b_2)^{\uparrow\downarrow}(3a_1)^{\uparrow\downarrow}(1b_1)^{0}+$	$1^1A'$:$C_1(1a')^{\uparrow\downarrow}(2a')^{\uparrow\downarrow}(3a')^{\uparrow\downarrow}(4a')^{\uparrow\downarrow}(1a'')^{0}+$
$C_2(1a_1)^{\uparrow\downarrow}(2a_1)^{\uparrow\downarrow}(1b_2)^{\uparrow\downarrow}(3a_1)^{0}(1b_1)^{\uparrow\downarrow}$	$C_2(1a')^{\uparrow\downarrow}(2a')^{\uparrow\downarrow}(3a')^{\uparrow\downarrow}(4a')^{0}(1a'')^{\uparrow\downarrow}$
$\widetilde{b}^1B_1$:$(1a_1)^{\uparrow\downarrow}(2a_1)^{\uparrow\downarrow}(1b_2)^{\uparrow\downarrow}(3a_1)^{\uparrow}(1b_1)^{\downarrow}$	$1^1A''$:$(1a')^{\uparrow\downarrow}(2a')^{\uparrow\downarrow}(3a')^{\uparrow\downarrow}(4a')^{\uparrow}(1a'')^{\downarrow}$
$\widetilde{c}^1A_1$:$C_3(1a_1)^{\uparrow\downarrow}(2a_1)^{\uparrow\downarrow}(1b_2)^{\uparrow\downarrow}(3a_1)^{\uparrow\downarrow}(1b_1)^{0}+$	$2^1A'$:$C_3(1a')^{\uparrow\downarrow}(2a')^{\uparrow\downarrow}(3a')^{\uparrow\downarrow}(4a')^{\uparrow\downarrow}(1a'')^{0}+$
$C_4(1a_1)^{\uparrow\downarrow}(2a_1)^{\uparrow\downarrow}(1b_2)^{\uparrow\downarrow}(3a_1)^{0}(1b_1)^{\uparrow\downarrow}$	$C_4(1a')^{\uparrow\downarrow}(2a')^{\uparrow\downarrow}(3a')^{\uparrow\downarrow}(4a')^{0}(1a'')^{\uparrow\downarrow}$
1^1A_2:$(1a_1)^{\uparrow\downarrow}(2a_1)^{\uparrow\downarrow}(1b_2)^{\uparrow}(3a_1)^{\uparrow\downarrow}(1b_1)^{\downarrow}$	$2^1A''$:$(1a')^{\uparrow\downarrow}(2a')^{\uparrow\downarrow}(3a')^{\uparrow}(4a')^{\uparrow\downarrow}(1a'')^{\downarrow}$
1^1B_2:$(1a_1)^{\uparrow\downarrow}(2a_1)^{\uparrow\downarrow}(1b_2)^{\uparrow}(3a_1)^{\downarrow}(1b_1)^{\uparrow\downarrow}$	$3^1A'$:$(1a')^{\uparrow\downarrow}(2a')^{\uparrow\downarrow}(3a')^{\uparrow}(4a')^{\downarrow}(1a'')^{\uparrow\downarrow}$

at linearity. The spin-orbit coupling between the $\widetilde{X}^3B_1$ and singlet states is small in the well region and thus is neglected in this work.

2.2. ab Initio Calculations. Two levels of *ab initio* calculations were performed for the PES construction which involves a dual-level strategy [43]. The electronic energies in the lower-level calculations are calculated with the state-averaged complete active space self-consistent field (SA-CASSCF) and internally contracted multireference configuration interaction (*ic*MRCI) methods [44–47]. The active space consists of six electrons distributed among seven orbitals, which correspond to all valence electrons and valence orbitals and one additional *3s* orbital of carbon which is of *Rydberg* character. The carbon *1s* orbital is not correlated but optimized at the SA-CASSCF level. To get a good description of the two lowest-lying singlet states, especially in view of the importance of correct degeneracy between $1^1A'$ and $1^1A''$ at linear geometries and the influence of PES intersections, we simultaneously consider the five singlet states which correlate with the C(^1D)+H_2 asymptote in the present *ab initio* calculations. Consequently, the SA-CASSCF calculations including three and two roots in the A' and A'' symmetries are carried out to obtain the orbitals for further *ic*MRCI calculations. The Davidson correction (denoted as +Q) is employed to include the correlation energy due to higher excitations. Dunning's correlation-consistent polarized valence quadruple-zeta basis set augmented with diffuse functions (*aug-cc-pVQZ*) is used.

In the higher-level calculations, the methods and algorithm are the same as the lower-level, but the active space and basis set are different. The active space consists of all electrons distributed among eight orbitals, which include 1s, all valence, and 3s orbital of carbon. The carbon *1s* orbital is correlated and also optimized at the SA-CASSCF level. To obtain the CV contribution to the energies, the *aug-cc-pVQZ* basis set for C atom is modified. The details of this scheme could be found elsewhere [42, 48–51], and only a brief outline will be given here. The seven inner *1s* functions are contracted to two functions using the coefficients from the *aug-cc-pVQZ* basis set. The outer five *s* functions are uncontracted as the six *p* functions. Two tight *d* and *f* functions are added to the (*3d, 2f, 1g*) polarized set given by Peterson and Dunning [42] and Woon and Dunning [48]. The additional functions are even tempered extensions of the valence sets, and the exponents of the added functions are 5.262 and 14.984 for the *d* functions and 4.152 and 12.147 for the *f* functions which are obtained by successively multiplying the corresponding tightest functions by the ratio of the first two compact functions [50, 51]. This core basis set, developed to treat both core and valence correlations, is of the form (*12s6p5d4f1g*)/[*7s6p5d4f1g*] and is designated as *optACVQZ*, which is much smaller than Dunning's standard *aug-cc-pCVQZ* [42, 48, 49] and gives a good description of core electrons [50, 51].

For the *ab initio* calculation of nonadiabatic terms, the SA-CASSCF method is used. The active space is the same as that of the lower-level energy calculations, and the basis set employed here is the uncontracted *aug-cc-pVQZ* basis. The nonadiabatic terms, required for calculating for the RT coupling, are the matrix elements of electronic orbital angular momentum $\hat{L}$, and they are obtained as expectation values over the SA-CASSCF wave functions. The RT coupling takes effect when the molecule approaches linearity, that is, lies on the z-axis, hence the matrix elements of $\hat{L}_x$ and $\hat{L}_y$ can be neglected. The details of the RT Hamiltonian have been discussed in another publication [52]. So, three matrix elements of electronic angular momentum (designated as L_z^{ab}, L_{zz}^{aa}, and L_{zz}^{bb}) are calculated, where $\langle \widetilde{a}^1A_1 \mid \hat{L}_z \mid \widetilde{b}^1B_1\rangle = -i\hbar L_z^{ab}$, $\langle \widetilde{a}^1A_1 \mid \hat{L}_z^2 \mid \widetilde{a}^1A_1\rangle = \hbar^2 L_{zz}^{aa}$, $\langle \widetilde{b}^1B_1 \mid \hat{L}_z^2 \mid \widetilde{b}^1B_1\rangle = \hbar^2 L_{zz}^{bb}$.

All *ab initio* calculations reported in the present work were carried out using the MOLPRO2006.1 package of *ab initio* programs [53].

2.3. PES Grid. In order to cover the region of spectroscopic interest with two deep potential wells, *ab initio* calculations at icMRCI(6e, 7o)+Q/AVQZ and *ic*MRCI(8e, 8o)+Q/*optACVQZ* levels were performed at 3042 and 273 symmetry unique geometries, respectively. These were chosen carefully to accurately represent the dynamically important regions, particularly the vicinities of the minimum and near linearity. As pointed out by Liu and co-workers [34], the $1^1\Pi$ pair ($3^1A'$ and $2^1A''$) states conically cross not only the $1^1\Delta$ pair ($1^1A'$ and $1^1A''$) states at around 3.4 bohr, but also the $1^1\Sigma_g^+$ state ($2^1A'$) at 3.1 bohr in the stretching potential curves of linear H–C–H (with one of the C–H bond lengths fixed at 2.1 bohr).

We concentrate on the geometries with the CH bond length smaller than 3.0 bohrs in the process of the present PES construction. Dozens of geometries are also selected for

the description of the higher energy regions. In the important regions, points were computed with small increments of 0.1–0.5 bohrs for bond length and 2.0–5.0° for bond angle, while in other regions coarser grids of 1.0-2.0 bohrs and 10.0–20.0° were used. Geometries with energies higher than 100 kcal/mol above the global minimum of $\tilde{a}^1A_1$ were not totally neglected but assigned a very small weight. In the calculations of *ic*MRCI(8e, 8o)/*optACVQZ*, the grids were chosen as the following: 1.4, 1.8, 2.0, 2.05, 2.2, 2.6, and 3.0 bohrs for CH distance; 80, 100, 120, 143, 155, 175, and 180° for ∠HCH. In the calculations for the nonadiabatic coupling terms, almost the same grids were selected as those used in the higher-level calculations.

3. Fit of the Potential Energy Surfaces

To construct the PESs for the $1^1A'$ and $1^1A''$ states of CH_2, we choose three-body expansion functional forms for the analytical representation of the PESs with respect to the internal coordinates (R_1, R_2, θ) using a dual-level strategy, and nonadiabatic coupling terms are also taken into account. The idea of the dual-level strategy is to use two levels of *ab initio* calculations so as to reduce the number of higher-level points needed for fitting [43], and the basic scheme is as follows. First, a set of lower-level *ab initio* points without the CV effect, which are calculated at the *ic*MRCI(6e, 7o)+Q/*AVQZ* level, is generated to construct a zeroth-order PES, V_x^0 ($x = a$, b stands for the $1^1A'$ and $1^1A''$ states of CH_2, resp.). Then, a set of higher-level points with the CV effect, calculated at the *ic*MRCI(8e, 8o)+Q/*optACVQZ* level, is generated, and the data set of the energy differences of the two levels is used to construct a surface, V_x^{core}. And it should be noted that the energies of the lower level are obtained from V_x^0, instead of the *ab initio* calculations. In addition, the nonadiabatic coupling terms, L_z^{ab}, L_{zz}^{aa}, and L_{zz}^{bb} ($\hbar = 1$ hereafter), are fitted into functions in the third stage for the future calculations. Each of these steps will now be described in more details as follows. The final adiabatic potential V is expressed as

$$V = V_x^0 + V_x^{\text{core}}. \tag{1}$$

By applying the Levenberg-Marquardt technique for the nonlinear optimization, it was found that there are numerical problems for $M \geq 11$ due to near linear dependence of the parameters, and thus quadruple precision arithmetic was needed to obtain convergence [54]. To improve the fit, energy points below 60 kcal/mol relative to the PES minimum are weighted by a factor of 100, and energy points over 100 kcal/mol are weighted by 0.1. To accurately fit the intersection seam of the two lowest-lying singlet PESs at the linear configurations, all the points with ∠HCH larger than 170° are weighted by a factor of 100.

3.1. Analytical Representation of V^0. For the analytical representation of V^0, the calculated energy points were fitted to a three-body expansion in curvilinear coordinates, which are believed to match the shape of the adiabatic PESs. For both electronic states, a Morse-type coordinate

$$\rho = 1 - e^{-\alpha(R-R_0)} \tag{2}$$

was used for the CH stretching mode, where $(R - R_0)$ is the displacement from the equilibrium geometry of the corresponding electronic state. For the angular coordinate, several types of polynomials were tested, including $\cos(\beta\theta)$, $\cos(\beta(\pi - \theta))$, $\cos(\beta(\theta - \theta_0))$, and $[(\theta - \theta_0) + \beta(\theta - \theta_0)^2 + \beta(\theta - \theta_0)^3]$. Finally, $\cos(\beta(\pi - \theta))$ was employed to describe the ∠HCH bending:

$$\begin{aligned} V_x^0 &= \sum_{ijk} C_{ijk}^x \rho_1^i \rho_2^j \rho_3^k \\ &= \sum_{ijk} C_{ijk}^x \left[1 - e^{-\alpha_1(R_1 - R_0^x)}\right]^i \left[1 - e^{-\alpha_2(R_2 - R_0^x)}\right]^j \\ &\quad \times [\cos(\beta(\pi - \theta))]^k. \end{aligned} \tag{3}$$

The parameters α_1, α_2, β, and the C_{ijk} are determined by performing unequally weighted least squares fit to the *ab initio* data.

3.2. Analytical Representation of V^{core}. The core correlation surface V^{core} was constructed in a similar way to the construction of V^0, and the surfaces can be expressed as

$$\begin{aligned} V_x^{\text{core}} &= C_{000}^x + \exp\left\{\alpha\left[(R_1 - R_0^x)^2 + (R_2 - R_0^x)^2\right]\right\} \\ &\quad \times \sum_{ijk} C_{ijk}^x \rho_1^i \rho_2^j \rho_3^k \\ &= C_{000}^x + \exp\left\{\alpha\left[(R_1 - R_0^x)^2 + (R_2 - R_0^x)^2\right]\right\} \\ &\quad \times \sum_{ijk} C_{ijk}^x \left[\frac{(R_1 - R_0^x)}{R_0^x}\right]^i \left[\frac{(R_1 - R_0^x)}{R_0^x}\right]^j \\ &\quad \times [\cos(\theta) - \cos(\theta_0^x)]^k. \end{aligned} \tag{4}$$

3.3. Analytical Representation of the Nonadiabatic Coupling Terms. To fit the matrix elements of $\hat{L}_z$ and $\hat{L}_z^2$ into analytical representations, several types of polynomials have been tested, and the following one provides a good description of the nonadiabatic coupling terms, L_z^{ab}, L_{zz}^{aa}, and L_{zz}^{bb}:

$$\begin{aligned} &C_{000} + \cos^2\left(\frac{\theta}{2}\right) \\ &\quad \times \sum_{ijk} C_{ijk}^n \left[1 - e^{-\alpha_1 R_1}\right]^i \left[1 - e^{-\alpha_2 R_2}\right]^j [\beta(\pi - \theta)]^k. \end{aligned} \tag{5}$$

In the analytical representation above, the $\cos^2(\theta/2)$ guarantees that L_{zz}^{aa} and L_{zz}^{bb} have a correct behavior at linearity. Several types of cos functions instead of $\beta(\pi - \theta)$ were tested as angular coordinate, but very good results were not obtained. $\beta(\pi - \theta)$ is found to be suitable for the description of the bending mode.

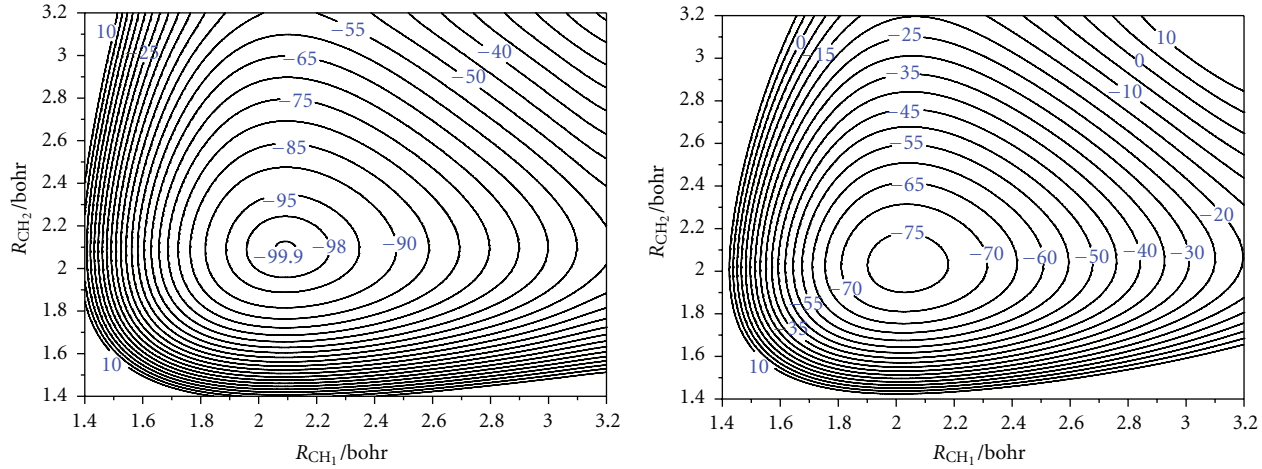

FIGURE 1: (a) Contour plot for the $1^1A'$ PES of CH_2 as a function of R_{CH_1} and R_{CH_2} (bohr) with ∠HCH fixed at the equilibrium value 102.45°. (b) Contour plot for the $1^1A''$ PES of CH_2 as a function of R_{CH_1} and R_{CH_2} (bohr) with ∠HCH fixed at the equilibrium value 144.36°. Energies (kcal/mol) are relative to the $C(^1D)+H_2$ asymptote.

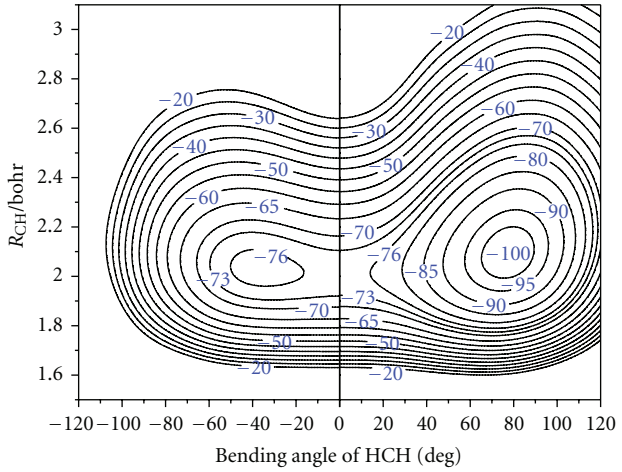

FIGURE 2: Contour plots for the $\tilde{a}^1A_1$ ($\rho \geq 0$) and $\tilde{b}^1B_1$ ($\rho \leq 0$) PESs as functions of R_{CH} and the bending angle of HCH. The intersection seam is shown as a bold line at $\rho = 0$, where ρ is the angle of bending. Energies (kcal/mol) are relative to the $C(^1D)+H_2$ asymptote.

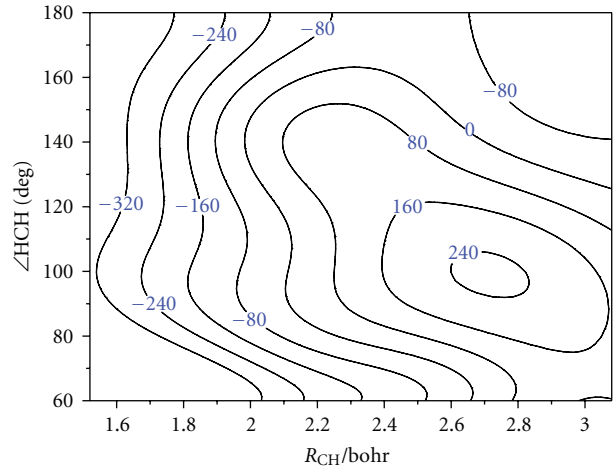

FIGURE 3: Contour plot (cm^{-1}) for V^{core} of the $\tilde{a}^1A_1$ state of CH_2 as a function of R_{CH} and ∠HCH.

Many test calculations were performed with different polynomial orders M, and the dependences are shown in Table S1 (see Table S1 in the Supplementary Material available online at doi: 10.1155/2012/236750). Although, the RMS errors in the fit become smaller as M goes higher, we choose $M = 10$ for the fit of V^0 due to numerical problems. The complete set of parameters amounts to a total of 286 linear coefficients and 3 nonlinear coefficients. The fit for V^0 has RMS errors of 31.88 and 142.88 cm^{-1} for the $1^1A'$ and $1^1A''$ states, respectively. Below 60 kcal/mol, the RMS errors are 6.64 and 5.94 cm^{-1}, respectively. In the fit of V^{core}, M is taken as 6. The complete set of parameters amounts to a total of 85 linear coefficients. The fit for V^{core} has RMS errors of 14.29 and 68.21 cm^{-1} for the $1^1A'$ and $1^1A''$ states, respectively. Below 60 kcal/mol, the RMS errors are 3.15 and 11.89 cm^{-1}, respectively. The numerical values of all parameters to generate the surfaces and coupling terms reported in the present study are presented in Tables S2, S3, and S4.

4. Features of the Fitted Surfaces and Vibronic Energy Level Calculations

4.1. Adiabatic PESs. Figure 1 presents the contour plots for CH bonds stretching of our PESs keeping ∠HCH fixed at 102.45° for the $\tilde{a}^1A_1$ state, 144.36° for the $\tilde{b}^1B_1$ state. We found the fitted potentials to be smooth and without any artificial oscillations. The degeneracy of the two lowest-lying singlet adiabatic potentials is illustrated in Figure 2.

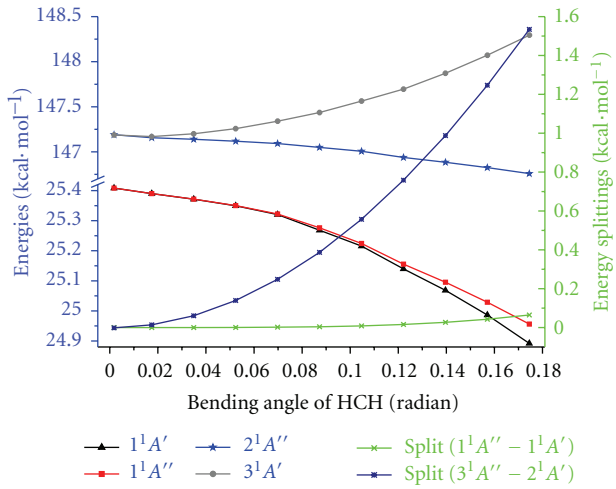

Figure 4: The bending potential energy curves for the four singlet states ($1^1A'$, $1^1A''$, $2^1A''$, and $3^1A'$) of CH_2 calculated at the *ic*MRCI(6e, 7o)+Q/*AVQZ* level. (The $2^1A'$ state, which lies between the $1^1A'$ and $3^1A'$ state, is not shown.) $R_{CH_1} = R_{CH_2} = 2.01$ bohrs. The zero energy is taken at the CH_2 ($1^1A'$) minimum.

They are contour plots as functions of R_{CH} and $\angle$HCH. Our fitted PESs for the two singlet states are degenerate at $R_{CH} = (1.6, 2.6)$ bohrs with $\angle$HCH = 180°. The PES difference at linear geometries in higher energy regions (with energies higher than 60 kcal/mol above the global minimum of $\tilde{a}^1A_1$) is due to the PES fitting error. To further improve the behavior of our PESs at linear geometries, we used an assumed angle dependence switching function to smoothly *connect* the two states above at linearity. Thus, this function is defined as follows:

$$f^{sw} = \frac{1}{2}\cos^4(\pi - \theta)\{1 - \tanh[200(1 + \cos\theta)]\}. \quad (6)$$

Two adiabatic potentials for the $\tilde{a}^1A_1$ and $\tilde{b}^1B_1$ states of CH_2, which are going to be degenerate at linearity, are represented as follows:

$$V_a = (V_a^0 + V_a^{core}) + \left[\left(V_b^0 + V_b^{core}\right) - (V_a^0 + V_a^{core})\right] f^{sw},$$
$$V_b = \left(V_b^0 + V_b^{core}\right) - \left[\left(V_b^0 + V_b^{core}\right) - (V_a^0 + V_a^{core})\right] f^{sw}. \quad (7)$$

From the experimental side, a wide number of studies have led to the determination of accurate equilibrium geometries for the $\tilde{a}^1A_1$ and $\tilde{b}^1B_1$ states of CH_2. Geometries and relative energies of minima obtained from our work along with the available experimental and other theoretical values are given in Table 2. We find the PES minimum of the $\tilde{a}^1A_1$ state on our PESs to be located at $R_{CH} = 2.092$ bohrs and $\angle$HCH = 102.45°. Obviously, these results are in very good agreement with the experimental value CH_2 available, $R_{CH} = 2.092 \pm 0.004$ bohrs and $\angle$HCH = 102.38°. Despite the ground singlet state being widely studied, there have been limited research on the first excited singlet state $\tilde{b}^1B_1$.

Table 2: Geometries and relative energies of the minima of the two lowest-lying singlet states of CH_2. R_e is the equilibrium interatomic distance, and θ_e is the equilibrium $\angle$HCH.

		Geometries		Relative energies (kcal·mol^{-1})*
		R_e (bohr)	θ_e (degree)	
$\tilde{a}^1A_1$	*Ab initio* without core[a]	2.0965	102.10	−100.54
	Ab initio with core[b]	2.0914	102.38	−100.70
	Our PESs[c]	2.0920	102.45	−100.70
	Liu et al.[d]	2.098	102.0	−100.3
	Flores and Gdanitz[e]	2.0917	102.31	
	Bussery-Honvault et al.[f]	2.09	102.5	−99.7
	DMBE[g]	2.09	102.4	−99.75
	Exp.[h]	2.099	102.38	
	Exp.[i]	2.092 ± 0.004	102.4 ± 0.4	
$\tilde{b}^1B_1$	*Ab initio* without core[a]	2.0316	143.12	−77.71
	Ab initio with core[b]	2.0300	144.60	−77.96
	Our PESs[c]	2.0300	144.36	−77.97
	Liu et al.[d]	2.032	143.2	−76.8
	Flores and Gdanitz[e]	2.0165	143.39	
	Bussery-Honvault et al.[f]	2.02	141	−79.9
	Exp.[h]	1.990	140 ± 15	
	Exp.[j]	2.052	139.30	

* Energies are relative to the $C(^1D)+H_2$ asymptote.
[a]Our *ab initio* values using *ic*MRCI(6e, 7o)+Q/*AVQZ*.
[b]Our *ab initio* values using *ic*MRCI(8e, 8o)+Q/*optACVQZ*.
[c]From our PESs.
[d]*Ab initio* values using *ic*MRCI(6e, 7o)/AVQZ from [34].
[e]*Ab initio* values using *ic*MR-ACPF(8e, 7o)/*ACVQZ* from [55].
[f]PES values from [27, 29].
[g]PES values from [30].
[h]Experimental values from [2].
[i]Experimental values from [11].
[j]Experimental values from [56].

As can be seen, this state is the open-shell singlet analog of the $\tilde{X}^3B_1$ state. As expected, its molecular orbitals and Mulliken atomic distributions are very similar to those of the ground state, which makes the *ab initio* calculation more difficult. The PES minimum for the $\tilde{b}^1B_1$ state on our PESs is located at $R_{CH} = 2.030$ bohrs and $\angle$HCH = 144.36°. In Figure 3, we have plotted the contours of the core corrections V^{core}, as functions of R_{CH} and $\angle$HCH of the $\tilde{a}^1A_1$ state. The CV effects have a geometry dependence, and the shifts can be positive or negative. The core correlations varies from −400 to 300 cm^{-1}. The inclusion of core and core-valence correlation decreases the bond lengths by 0.0051 and 0.0016 bohrs and increases the bond angle by 0.28 and 1.48° for the $\tilde{a}^1A_1$ and $\tilde{b}^1B_1$ states, respectively.

The $1^1\Delta_g$ state of HCH at linear configuration, splitting into the two lowest-lying singlet electronic excited states

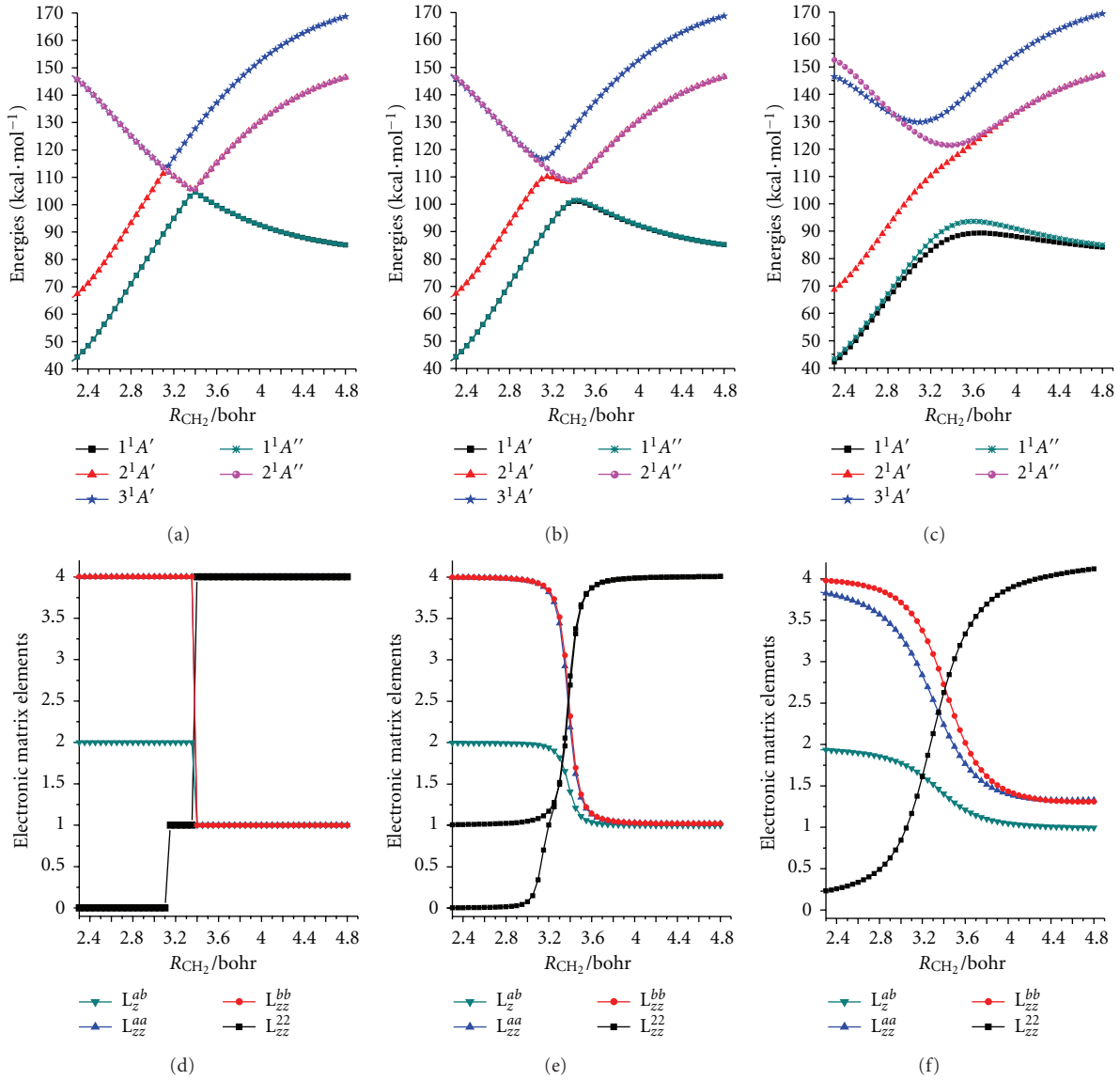

FIGURE 5: The stretching potential curves of the five singlet states ($1^1A'$, $2^1A'$, $3^1A'$, $1^1A''$, and $2^1A''$ state) of CH_2 as functions of the bond length R_{CH_2} with the ∠HCH fixed at (a) 180°, (b) 175°, and (c) 160°, respectively; The Renner-Teller terms L_z^{ab}, L_{zz}^{aa}, L_{zz}^{bb}, and L_{zz}^{22} ($\langle 2^1A' \mid \hat{L}_z^2 \mid 2^1A' \rangle$) as functions of the bond length R_{CH_2} with ∠HCH fixed at (d) 180°, (e) 175°, and (f) 160°, respectively. R_{CH_1} is fixed at 2.09 bohrs, and the zero energy is taken at the CH_2 ($1^1A'$) minimum.

$\tilde{a}^1A_1$ and $\tilde{b}^1B_1$ as the molecule is bent, is a prime example of the vibronic RT effect. In this case, the splitting will be proportional to ρ^n, where $n = 2\Lambda$ and Λ (Λ= 1 for Π, and 2 for Δ state) is the eigenvalue of $\hat{L}_z$, the axial component of electronic angular momentum at linearity. Although the other two higher excited states ($3^1A'$ and $2^1A''$) calculated with *ic*MRCI(6e, 7o)+Q/*AVQZ* are not involved in the present PESs, it is clearly seen that in this region the *ab initio* computed PECs show the ρ^2 behavior for the doubly degenerate Π pair ($3^1A'$ and $2^1A''$) in Figure 4. The energy splittings between $1^1\Delta_g$ pair and $1^1\Pi_g$ pair states go quartically and quadratically, respectively, when approaching linearity.

While the energy changes with the CH bond stretched, the degeneracy of the $1^1A'$ and $1^1A''$ (or $3^1A'$ and $2^1A''$) of CH_2 is not lifted so long as the molecule is linear. The barrier to linearity plays a very important role in quantum mechanical calculations of vibronic energy levels when the RT effect is considered [18]. The height of the barrier to linearity in $\tilde{a}^1A_1$ CH_2 has been a long standing source of controversy. The range of reported barrier heights for linearity in the $\tilde{a}^1A_1$ state of CH_2 is quite large, varying from 8000 to 10000 cm^{-1}, which is summarized in Table 3. Herzberg and Johns originally gave a value of 8000 cm^{-1}, estimated from the spacing of the $\tilde{b}^1B_1$ bending vibrational levels [2]. Duxbury and Jungen [56] obtained a barrier of

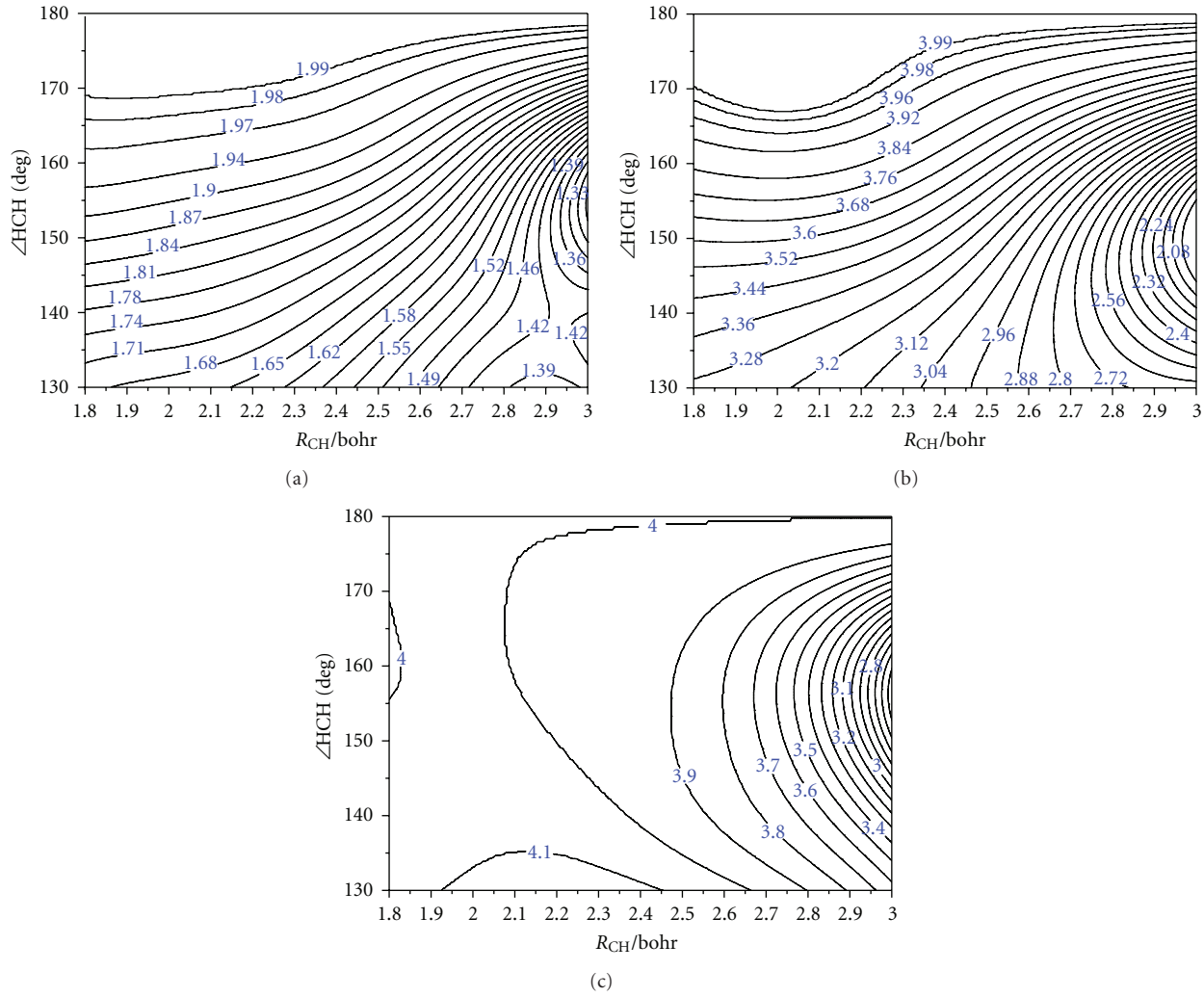

FIGURE 6: Contour plots for the Renner-Teller terms of CH_2 for the two lowest-lying singlet electronic states as functions of R_{CH} and ∠HCH: (a) L_z^{ab}, (b) L_{zz}^{aa}, and (c) L_{zz}^{bb}.

9800 cm^{-1} by fitting a bending potential function to the $(0, v_2, 0)$ levels. An earlier *ab initio* calculation gave a barrier height of 9600 cm^{-1} [57]. Kalemos et al. [3] calculated this value to be 9217.7 cm^{-1}. In 2009, the DMBE PES predicted 9644 cm^{-1} in agreement with the experimental determination of 9800 cm^{-1} [56].

Green Jr. et al. [17] calculated an *ab initio* value of 9125 cm^{-1} and empirically adjusted it to about 8800 cm^{-1} according to the visible spectra around 15000 cm^{-1}. And this value is in very good agreement with the derived value of 8600 ± 400 cm^{-1} from the experiment by Hartland et al. [8]. The value of 8666 cm^{-1} was obtained from the PESs constructed by Gu et al. [19] via fitting experimental data and a few *ab initio* points. Liu et al. gave the value as 8797 cm^{-1} based upon the *ic*MRCI(6e, 7o)+Q/*AVQZ* calculations with three reference states in the A' symmetry. Our *ab initio* calculation at the same level with five reference states gives the barrier to linearity as 8895.1 cm^{-1}, but when the core correlation is taken into account, we obtain the *ab initio* calculated barrier to linearity as 8735.8 cm^{-1}. The core correlations reduce this value by 160 cm^{-1}. It may be due to the fact that the *1s* electron is affected when the valence orbitals change from sp^2 hybridization at the minimum area to *sp* hybridization at linearity. Our PESs predict a height of 8715.02 and 760.2 cm^{-1} for the barriers to linearity in the $\tilde{a}^1A_1$ and $\tilde{b}^1B_1$ states of CH_2, respectively.

4.2. Renner-Teller Nonadiabatic Coupling Terms. The fit of the RT nonadiabatic coupling terms has an RMS error of 0.0060, 0.0225, and 0.0148 for L_z^{ab}, L_{zz}^{aa}, and L_{zz}^{bb}, respectively. The polynomial order M is taken as 9. Note that $\langle 1^1A'|\hat{L}_z|1^1A''\rangle$ is imaginary and its absolute value is thus used. Figures 5(a), 5(b), and 5(c) describe the stretching potential curves of the five singlet states ($1^1A'$, $2^1A'$, $3^1A'$, $1^1A''$ and $2^1A''$ state) of CH_2 as functions of bond length R_{CH_2}, with R_{CH_1} fixed at 2.09 bohrs and ∠HCH at 180°, 175° and 160°, respectively; at linearity, $1^1A'$ and $1^1A''$ states become a degenerate Δ pair. Due to the conical intersection between Π and Δ at R_{CH_2} = 3.38 bohrs, L_z^{ab}, L_{zz}^{aa}, and L_{zz}^{bb} in

Table 3: The barrier to linearity of the $\widetilde{a}^1A_1$ and $\widetilde{b}^1B_1$ states.

Barrier to linearity		Note
$\widetilde{a}^1A_1$ (cm^{-1})	$\widetilde{b}^1B_1$ (cm^{-1})	
9073.5	885.2	Our calculation at *ic*MRCI(6e, 7o)/*AVQZ*
8895.1	907.3	Our calculation at *ic*MRCI(6e, 7o)+Q/*AVQZ*
8735.8	706.2	Our calculation at *ic*MRCI(8e, 8o)+Q/*optACVQZ*
8715.1	760.2	Our PESs
8800		The empirically adjusted value based on the visible spectra[a]
8797		*Ab initio* value[b]
8666	725	The fit of empirically spectra and *ab initio* calculations[c]
8600 ± 400		The derived value from experiment[d]
8000		The derived value from experiment[e]
9217.7	953.2	*Ab initio* value[f]
9644		*Ab initio* value[g]
9451.1	1193.0	Others[h]
9750.0 ± 71.0	1616.6 ± 94	Others[i]
9600		Others[j]
9870		Others[k]
9144	879	Others[l]
9356	1049	Others[m]

[a]From Ref. [17]. [b]From [34]. [c]From [8]. [d]From [19]. [e]From [2]. [f]From [3]. [g]From [30]. [h]From [5]. [i]From [56]. [j]From [57]. [k]From [7]. [l]From [41].[m]From [24].

Figure 5(d), which shows the dependence of the electronic matrix elements with R_{CH_2} stretching, are almost constants (2, 4, and 4) for $R_{CH_2} < 3.38$ bohrs due to quantization of the electronic angular momenta ($L_z^{ab} = 2$, $L_{zz}^{aa,bb} = 4$ for the Δ state); however, they change rapidly to 1 at $R_{CH_2} \approx 3.38$ bohrs. Almost similar changing could be found in Figures 5(e) and 5(f) with $\angle$HCH = 175 and 160° due to the PESs intersections. And much more interesting rapid changing can also be found in the other three states ($2^1A'$, $3^1A'$, and $2^1A''$), for example, $\langle 2^1A' \mid \hat{L}_z^2 \mid 2^1A' \rangle$, but this is beyond the subject of the present work.

In Figure 6, the contour plots for L_z^{ab}, L_{zz}^{aa}, and L_{zz}^{bb} of the $\widetilde{a}^1A_1$ and $\widetilde{b}^1B_1$ states of CH_2 as function of CH stretching and $\angle$HCH bending are presented. It is well noticed that along the HCH axis, the values of $L_z^{ab} \simeq 2$ and $L_{zz}^{aa,bb} \simeq 4$ but then as the molecule deviates from linearity the values of L_z^{ab} and L_{zz}^{aa} decrease, and the values of L_{zz}^{bb} increase at the short R_{CH} region but decrease at the long R_{CH} region. The values of L_z^{ab} and $L_{zz}^{aa,bb}$ begin to drop rapidly and monotonically to 1 at $R_{CH} = 3.1$ bohrs due to the Δ/Π PES intersection at linearity. Figure 7 shows the variation of the electronic matrix elements for the two lowest-lying singlet electronic states as functions of the bending angle $\angle$HCH, with the CH-distance optimized for the $\widetilde{a}^1A_1$ state. It is shown that, as the molecule bends, the curve of L_z^{ab} decreases monotonically from 2, that of L_{zz}^{bb} rises from 4 basically in a monotonic way, but that of L_{zz}^{aa} first goes down from 4 and then goes up.

Table 4: The calculated $J = 0$ vibronic energy levels of the $\widetilde{a}^1A_1$ and $\widetilde{b}^1B_1$ states on our *ab initio* PESs employing the MCTDH method, compared with other theoretical results and experimental values. The energy levels are in cm^{-1}, relative to the zero point energy of the $\widetilde{a}^1A_1$ state.

$\widetilde{a}/\widetilde{b}$	ν_1	ν_2	ν_3	Green Jr. et al.[a]	Gu et al.[b]	Ours	Expt.
$\widetilde{a}$	0	1	0	1356	1351.2	1350.9	1352.6[d]
$\widetilde{a}$	0	2	0	2675	2664.1	2666.9	2667.7[d]
$\widetilde{a}$	1	0	0	2808	2807.5	2808.9	2806.0[e]
$\widetilde{a}$	0	0	1	2863	2864.5	2862.5	2865.0[e]
$\widetilde{a}$	0	3	0	3962	3945.6	3950.6	3950.5[d]
$\widetilde{a}$	1	1	0	4159	4156.5	4150.4	4152.8[f]
$\widetilde{a}$	0	4	0	5216	5191.5	5199.2	5196.6[d]
$\widetilde{a}$	1	2	0	5452	5437.6	5444.1	5444.9[f]
$\widetilde{a}$	2	0	0	5538	5529.3	5529.3	5531.4[f]
$\widetilde{a}$	0	5	0	6430	6397.9	6406.8	6403.0[d,f]
$\widetilde{a}$	1	3	0		6706.4	6712.0	6714.1[f]
$\widetilde{b}$	0	0	0	8383	8354	8349	8350[h]
$\widetilde{b}$	0	1	0	9566	9537	9534	9537[h]
$\widetilde{b}$	0	2	0	10848	10831	10828	10827[h,i]
$\widetilde{b}$	0	3	0	12231	12226	12220	12220[g,i,j]
$\widetilde{b}$	0	4	0	13681	13684	13673	13678[g]
$\widetilde{b}$	1	2	0	13850	13840	13835	13834[g]
$\widetilde{b}$	1	3	0	15116	15121	15106	15114[g]
$\widetilde{b}$	0	5	0	15317	15326	15313	15319[g]
$\widetilde{b}$	2	2	0	16749	16749	16738	16742[k]
$\widetilde{b}$	0	6	0	16929	16948	16934	16941[c,g]
$\widetilde{b}$	1	5	0	18186	18201	18182	18192[k]
$\widetilde{b}$	0	7	0	18590	18617	18603	18610[c,g]

[a]From [17]. [b]From [19].[c]From [58]. [d]From [8]. [e]From [11]. [f]From [59]. [g]From [2]. [h]From [10]. [i]From [12]. [j]From [9]. [k]From [60].

4.3. Vibronic Energy Level Calculations. We have calculated the vibronic energy levels of the $\widetilde{a}^1A_1$ and $\widetilde{b}^1B_1$ states on our *ab initio* PESs employing the block improved relaxation scheme [61, 62] in the multiconfiguration time-dependent Hartree (MCTDH) method [63–65]. The $J = 0$ energy results are listed in Table 4 and are compared with experiments and calculations by other groups. The variation of the electronic matrix elements with geometry is not considered, and other groups also adopted this treatment in previous calculations. For consistency, the energy levels in Table 4 are labeled by the bent molecular notation (ν_1, ν_2, ν_3).

Our calculated results are in excellent agreement with the experimental values, reflecting the accuracy of the constructed *ab initio* PESs. For the energy level of $\widetilde{b}(0, 2, 0)$, our result 10828 cm^{-1} is closer to the experimental value 10827 cm^{-1} from Sears et al. [10, 12] than 10823 cm^{-1} from Herzberg and Johns [2]. The experimental results from Sears et al. are more reliable [10, 12, 16]. Compared with the

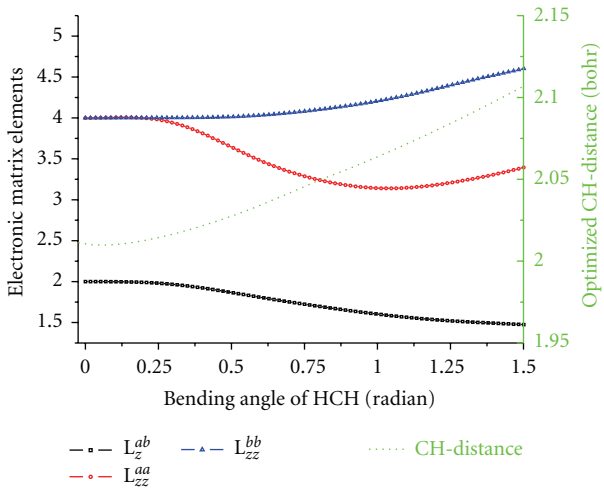

FIGURE 7: The Renner-Teller terms (L_z^{ab}, L_{zz}^{aa}, and L_{zz}^{bb}) of CH_2 for the two lowest-lying singlet electronic states as functions of the bending angle ∠HCH, with the CH-distance optimized for the $\tilde{a}^1A_1$ state.

calculated results from Green Jr. et al., our results are closer to experiment [17]. Generally speaking, our results are in slightly better agreement with the experimental values than the results of Gu et al. [19], and it should be noted that the semiempirical PESs used by Gu et al. were adjusted according to the experimental values while ours are fully *ab initio* ones.

5. Summary

In this work, we report fully *ab initio* PESs for the RT coupled $1^1A'$ and $1^1A''$ states of CH_2 suitable for the spectroscopic study, based on the *ic*MRCI+Q method using the *AVQZ* and a kind of optimized *ACVQZ* basis sets. The core and core-valence correlation effects are included, which are necessary for an accurate quantum chemical description of the CH_2 electronic states. The analytical representations of the two lowest-lying singlet PESs, with the inclusion of the matrix elements of electronic angular momentum L_z^{ab}, L_{zz}^{aa}, and L_{zz}^{bb}, are obtained by fitting. The obtained PESs are smooth, and the two adiabatic potentials are exactly degenerate at linearity. The minimal energy structures and the barriers to linearity predicted by our PESs are in excellent agreement with available experimental data. Furthermore, the MCTDH quantum dynamical calculations are carried out on these new PESs, and the calculated vibronic energy levels are in excellent agreement with the experimental values. Further work on the construction of the global PESs for the $1^1A'$ and $1^1A''$ states, suitable for the $C(^1D)+H_2$ reactive scattering studies, is in progress, and various PES intersections as revealed in our previous work [34], in particular conical intersections, will be included.

Acknowledgments

This work is supported by National Natural Science Foundation of China (nos. 20733005 and 21173232), Chinese Academy of Sciences, and Beijing National Laboratory for Molecular Sciences. The authors would like to thank Professor H. Partridge for useful discussions of the modified basis set *optACVQZ* for core-valence calculations.

References

[1] R. A. Beärda, M. C. Van Hemert, and E. F. Van Dishoeck, "Photodissociation of CH_2. I. Potential energy surfaces of the dissociation into CH and H," *The Journal of Chemical Physics*, vol. 97, no. 11, pp. 8240–8249, 1992.

[2] G. Herzberg and J. W. C. Johns, "The Spectrum and Structure of Singlet CH_2," *Proceedings of the Royal Society of London A*, vol. 295, no. 1441, pp. 107–128, 1966.

[3] A. Kalemos, T. H. Dunning, A. Mavridis, and J. F. Harrison, "CH_2 revisited," *Canadian Journal of Chemistry*, vol. 82, no. 6, pp. 684–693, 2004.

[4] C. D. Sherrill, M. L. Leininger, T. J. V. Huis, and H. F. Schaefer III, "Structures and vibrational frequencies in the full configuration interaction limit: predictions for four electronic states of methylene using a triple-zeta plus double polarization (TZ2P) basis," *The Journal of Chemical Physics*, vol. 108, no. 3, pp. 1040–1049, 1998.

[5] M. N. R. Ashfold, M. A. Fullstone, G. Hancock, and G. Duxbury, "Laser induced fluorescence spectroscopy of the CD_2 ($\tilde{a}^1A_1$) radical: Renner-teller effect in CH_2 and CD_2," *Molecular Physics* , vol. 45, no. 4, pp. 887–896, 1982.

[6] W. Xie, C. Harkin, H. L. Dai, W. H. Green, Q. K. Zheng, and A. J. Mahoney, "Transient vibrational spectroscopy of $\tilde{a}^1A_1$ CH_2 $v_2 = 2$," *Journal of Molecular Spectroscopy*, vol. 138, no. 2, pp. 596–601, 1989.

[7] W. Xie, C. Harkin, and H. L. Dai, "Bending overtones and barrier height of $\tilde{a}^1A_1$ CH_2 by flash photolysis stimulated emission pumping," *The Journal of Chemical Physics*, vol. 93, no. 7, pp. 4615–4623, 1990.

[8] G. V. Hartland, D. Qin, and H. L. Dai, "Renner-Teller effect on the highly excited bending levels of $\tilde{a}^1A_1$ CH_2 ," *The Journal of Chemical Physics*, vol. 102, no. 17, pp. 6641–6645, 1995.

[9] B. C. Chang, M. Wu, G. E. Hall, and T. J. Sears, "Near-infrared vibronic spectrum of the CH_2 $\tilde{b}^1B_1 \leftarrow \tilde{a}^1A_1$ transition," *The Journal of Chemical Physics*, vol. 101, no. 11, pp. 9236–9245, 1994.

[10] K. Kobayashi, L. D. Pride, and T. J. Sears, "Absorption spectroscopy of singlet CH_2 near 9500 cm^{-1}," *The Journal of Physical Chemistry A*, vol. 104, no. 45, pp. 10119–10124, 2000.

[11] H. Petek, D. J. Nesbitt, D. C. Darwin, P. R. Ogilby, C. B. Moore, and D. A. Ramsay, "Analysis of CH_2 $\tilde{a}^1A_1$ (1,0,0) and (0,0,1) Coriolis-coupled states, $\tilde{a}^1A_1$-$\tilde{x}^3B_1$ spin-orbit coupling, and the equilibrium structure of CH_2 $\tilde{a}^1A_1$," *The Journal of Chemical Physics*, vol. 91, no. 11, pp. 6566–6578, 1989.

[12] G. E. Hall, A. V. Komissarov, and T. J. Sears, "Doppler-resolved spectroscopy as an assignment tool in the spectrum of singlet methylene," *The Journal of Physical Chemistry A*, vol. 108, no. 39, pp. 7922–7927, 2004.

[13] A. J. Marr, T. J. Sears, and B. C. Chang, "Near-infrared spectroscopy of CH_2 by frequency modulated diode laser absorption," *The Journal of Chemical Physics*, vol. 109, no. 9, pp. 3431–3442, 1998.

[14] Z. Wang, Y. Kim, G. E. Hall, and T. J. Sears, "State mixing and predissociation in the $\tilde{c} \leftarrow \tilde{a}$ band system of singlet methylene studied by optical-optical double resonance," *The Journal of Physical Chemistry A*, vol. 112, no. 39, pp. 9248–9254, 2008.

[15] K. Kobayashi, G. E. Hall, and T. J. Sears, "The spectrum of CH_2 near 1.36 and 0.92 μm: reevaluation of rotational level structure and perturbations in $\tilde{a}(010)$," *The Journal of Chemical Physics*, vol. 124, no. 18, Article ID 184320, 2006.

[16] C. -H. Chang, Z. Wang, G. E. Hall, T. J. Sears, and J. Xin, "Transient laser absorption spectroscopy of CH_2 near 780 nm," *Journal of Molecular Spectroscopy*, vol. 267, no. 1-2, pp. 50–57, 2011.

[17] W. H. Green Jr., N. C. Handy, P. J. Knowles, and S. Carter, "Theoretical assignment of the visible spectrum of singlet methylene," *The Journal of Chemical Physics*, vol. 94, no. 1, pp. 118–132, 1991.

[18] G. Duxbury, A. Alijah, B. D. McDonald, and C. Jungen, "Stretch-bender calculations of the effects of orbital angular momentum and vibrational resonances in the spectrum of singlet methylene," *The Journal of Chemical Physics*, vol. 108, no. 6, pp. 2351–2360, 1998.

[19] J. P. Gu, G. Hirsch, R. J. Buenker et al., "A theoretical study of the absorption spectrum of singlet CH_2 ," *Journal of Molecular Structure*, vol. 517-518, pp. 247–264, 2000.

[20] R. Renner, "Zur Theorie der Wechselwirkung zwischen Elektronen- und Kernbewegung bei dreiatomigen, stabförmigen Molekülen," *Zeitschrift für Physik*, vol. 92, no. 3-4, pp. 172–193, 1934.

[21] G. J. Halasz, A. Vibok, R. Baer, and M. Baer, "Renner-Teller nonadiabatic coupling terms: an *ab-initio* study of the HNH molecule," *The Journal of Chemical Physics*, vol. 124, no. 8, Article ID 081106, 4 pages, 2006.

[22] G. J. Halász, Á. Vibók, R. Baer, and M. Baer, "D matrix analysis of the Renner-Teller effect: an accurate three-state diabatization for NH_2," *The Journal of Chemical Physics*, vol. 125, no. 9, Article ID 094102, 9 pages, 2006.

[23] S. Zhou, Z. Li, D. Xie, S. Y. Lin, and H. Guo, "An *ab initio* global potential-energy surface for NH_2 (A^2A') and vibrational spectrum of the Renner-TellerA^2A'-X^2A'' system," *The Journal of Chemical Physics*, vol. 130, no. 18, Article ID 184307, 10 pages, 2009.

[24] G. Duxbury, B. D. McDonald, M. Van Gogh, A. Alijah, C. Jungen, and H. Palivan, "The effects of vibrational resonances on Renner-Teller coupling in triatomic molecules: the stretch-bender approach," *The Journal of Chemical Physics*, vol. 108, no. 6, pp. 2336–2350, 1998.

[25] C. Jungen, D. N. Malm, and A. J. Merer, "Analysis of a $^1\Delta_u - {}^1\Sigma_g{}^+$ transition of CS_2 in the near ultraviolet," *Canadian Journal of Physics*, vol. 51, no. 14, pp. 1471–1490, 1973.

[26] B. Ostojić, "The dissociation of singlet methylene," *Journal of Molecular Spectroscopy*, vol. 212, no. 1, pp. 130–131, 2002.

[27] B. Bussery-Honvault, P. Honvault, and J. M. Launay, "A study of the $C(^1D) + H_2 \rightarrow CH + H$ reaction: global potential energy surface and quantum dynamics," *The Journal of Chemical Physics*, vol. 115, no. 23, pp. 10701–10708, 2001.

[28] L. Bañares, F. J. Aoiz, P. Honvault, B. Bussery-Honvault, and J. M. Launay, "Quantum mechanical and quasi-classical trajectory study of the $C(^1D) + H_2$ reaction dynamics," *The Journal of Chemical Physics*, vol. 118, no. 2, pp. 565–568, 2003.

[29] B. Bussery-Honvault, J. Julien, P. Honvault, and J.-M. Launay, "Global 1 1A″ potential energy surface of CH_2 and quantum dynamics of a sideways insertion mechanism for the $C(^1D) + H_2 \rightarrow CH(^2\Pi) + H$ reaction," *Physical Chemistry Chemical Physics*, vol. 7, no. 7, pp. 1476–1481, 2005.

[30] S. Joseph and J. C. Varandas, "Accurate double many-body expansion potential energy surface for the lowest singlet state of methylene," *The Journal of Physical Chemistry A*, vol. 113, no. 16, pp. 4175–4183, 2009.

[31] A. J. C. Varandas, "Intermolecular and intramolecular potentials: topographical aspects, calculation, and functional representation via a double many-body expansion method," *Advances in Chemical Physics*, vol. 74, pp. 255–338, 1988.

[32] S. Joseph, P. J. S. B. Caridade, and A. J. C. Varandas, "Quasiclassical trajectory study of the $C(^1D) + H_2$ reaction and isotopomeric variants: kinetic isotope effect and cd/ch branching ratio," *The Journal of Physical Chemistry A*, vol. 115, no. 27, pp. 7882–7890, 2011.

[33] R. Dawes, A. F. Wagner, and D. L. Thompson, "Ab initio wavenumber accurate spectroscopy: $^1CH_2$ and HCN vibrational levels on automatically generated IMLS potential energy surfaces," *The Journal of Physical Chemistry A*, vol. 113, no. 16, pp. 4709–4721, 2009.

[34] X. Liu, W. Bian, X. Zhao, and X. Tao, "Potential energy surface intersections in the $C(^1D)H_2$ reactive system," *The Journal of Chemical Physics*, vol. 125, Article ID 074306, 7 pages, 2006.

[35] H. Zhao, W. Bian, and K. Liu, "A theoretical study of the reaction of $O(^3P)$ with isobutene," *Journal of Physical Chemistry A*, vol. 110, no. 25, pp. 7858–7866, 2006.

[36] N. Matsunaga and D. R. Yarkony, "Energies and derivative couplings in the vicinity of a conical intersection. II. $CH_2(2^3A'',3^3A'')$ and $H_2S(1^1A''2^1A'')$, unexpected results in an ostensibly standard case," *The Journal of Chemical Physics*, vol. 107, no. 19, pp. 7825–7838, 1997.

[37] D. R. Yarkony, "Diabolical conical intersections," *Reviews of Modern Physics*, vol. 68, no. 4, pp. 985–1013, 1996.

[38] J. Ivanic, G. J. Atchity, and K. Ruedenberg, "Violation of the weak noncrossing rule between totally symmetric closed-shell states in the valence-isoelectronic series O_3, S_3, SO_2, and S_2O," *The Journal of Chemical Physics*, vol. 107, no. 11, pp. 4307–4317, 1997.

[39] G. J. Atchity and K. Ruedenberg, "Strong shifts in diabatic nondynamic electron correlations cause conical intersection between low-lying closed-shell adiabatic singlets of like symmetry in ozone," *The Journal of Chemical Physics*, vol. 99, no. 5, pp. 3790–3798, 1993.

[40] H. Ma, X. Liu, W. Bian, L. Meng, and S. Zheng, "A theoretical study of the mechanism and kinetics of $F + N_3$ reactions," *ChemPhysChem*, vol. 7, no. 8, pp. 1786–1794, 2006.

[41] P. Jensen, M. Brumm, W. P. Kraemer, and P. R. Bunker, "A treatment of the Renner effect using the MORBID hamiltonian," *Journal of Molecular Spectroscopy*, vol. 171, no. 1, pp. 31–57, 1995.

[42] K. A. Peterson and T. H. Dunning, "Accurate correlation consistent basis sets for molecular core-valence correlation effects: the second row atoms Al-Ar, and the first row atoms B-Ne revisited," *The Journal of Chemical Physics*, vol. 117, no. 23, pp. 10548–10560, 2002.

[43] J. Cao, Z. Zhang, C. Zhang, W. Bian, and Y. Guo, "Kinetic study on the $H+SiH_4$ abstraction reaction using an *ab initio* potential energy surface," *The Journal of Chemical Physics*, vol. 134, no. 2, 2011.

[44] H. J. Werner and P. J. Knowles, "A second order multiconfiguration SCF procedure with optimum convergence," *The Journal of Chemical Physics*, vol. 82, no. 11, pp. 5053–5063, 1985.

[45] H. J. Werner and W. Meyer, "A quadratically convergent multiconfiguration-self-consistent field method with simultaneous optimization of orbitals and Cl coefficients," *The Journal of Chemical Physics*, vol. 73, no. 5, pp. 2342–2356, 1980.

[46] H. J. Werner and W. Meyer, "A quadratically convergent MCSCF method for the simultaneous optimization of several

states," *The Journal of Chemical Physics*, vol. 74, no. 10, pp. 5794–5801, 1981.

[47] H. J. Werner and P. J. Knowles, "An efficient internally contracted multiconfiguration-reference configuration interaction method," *The Journal of Chemical Physics*, vol. 89, no. 9, pp. 5803–5814, 1988.

[48] D. E. Woon and T. H. Dunning, "Gaussian basis sets for use in correlated molecular calculations. V. Core-valence basis sets for boron through neon," *The Journal of Chemical Physics*, vol. 103, no. 11, pp. 4572–4585, 1995.

[49] A. K. Wilson, T. Van Mourik, and T. H. Dunning, "Gaussian basis sets for use in correlated molecular calculations. VI. Sextuple zeta correlation consistent basis sets for boron through neon," *Journal of Molecular Structure: THEOCHEM*, vol. 388, no. 1–3, pp. 339–349, 1996.

[50] H. Partridge and D. W. Schwenke, "The determination of an accurate isotope dependent potential energy surface for water from extensive *ab initio* calculations and experimental data," *The Journal of Chemical Physics*, vol. 106, no. 11, pp. 4618–4639, 1997.

[51] O. L. Polyansky, A. G. Császár, S. V. Shirin et al., "High-accuracy *ab initio* rotation-vibration transitions for water," *Science*, vol. 299, no. 5606, pp. 539–542, 2003.

[52] Z. Zhang, H. Ma, and W. Bian, "Accurate quantum mechanical study of the Renner-Teller effect in the singlet CH_2 ," *The Journal of Chemical Physics*, vol. 135, Article ID 154303, 10 pages, 2011.

[53] H.-J. Werner, P. J. Knowles, R. Lindh et al., MOLPRO, version 2006.1, a package of *ab initio* programs.

[54] W. Bian and H.-J. Werner, "Global *ab initio* potential energy surfaces for the CIH_2 reactive system," *The Journal of Chemical Physics*, vol. 112, no. 1, pp. 220–229, 2000.

[55] J. R. Flores and R. J. Gdanitz, "Accurately solving the electronic Schrödinger equation of small atoms and molecules using explicitly correlated (r_{12}-)MR-CI. VIII. Valence excited states of methylene (CH_2)," *The Journal of Chemical Physics*, vol. 123, no. 14, Article ID 144316, 8 pages, 2005.

[56] G. Duxbury and C. Jungen, "Effects of orbital angular momentum in CH_2 The Renner-Teller effect," *Journal of Polymer Science B*, vol. 63, no. 6, pp. 981–998, 1988.

[57] D. C. Comeau, I. Shavitt, P. Jensen, and P. R. Bunker, "An *ab initio* determination of the potential-energy surfaces and rotation-vibration energy levels of methylene in the lowest triplet and singlet states and the singlet—triplet splitting," *The Journal of Chemical Physics*, vol. 90, no. 11, pp. 6491–6500, 1989.

[58] H. Petek, D. J. Nesbitt, D. C. Darwin, and C. Bradley Moore, "Visible absorption and magnetic−rotation spectroscopy of $^1CH_2$: The analysis of the $\tilde{b}^1B_1$ state ," *The Journal of Chemical Physics*, vol. 86, no. 3, pp. 1172–1188, 1987.

[59] G. V. Hartland, D. Qin, and H. L. Dai, "Fourier transform dispersed fluorescence spectroscopy: observation of new vibrational levels in the 5000–8000 cm^{-1} region of $\tilde{a}^1A_1$ CH_2 ," *The Journal of Chemical Physics*, vol. 98, no. 3, pp. 2469–2472, 1993.

[60] W. H. Green, I. C. Chen, H. Bitto, D. R. Guyer, and C. B. Moore, "New vibrational bands of CH_2 ($\tilde{b}^1B_1$)," *Journal of Molecular Spectroscopy*, vol. 138, no. 2, pp. 614–629, 1989.

[61] L. J. Doriol, F. Gatti, C. Iung, and H. D. Meyer, "Computation of vibrational energy levels and eigenstates of fluoroform using the multiconfiguration time-dependent Hartree method," *The Journal of Chemical Physics*, vol. 129, no. 22, Article ID 224109, 9 pages, 2008.

[62] H. D. Meyer, F. L. Quéré, C. Léonard, and F. Gatti, "Calculation and selective population of vibrational levels with the Multiconfiguration Time-Dependent Hartree (MCTDH) algorithm," *Chemical Physics*, vol. 329, no. 1-3, pp. 179–192, 2006.

[63] H.-D. Meyer, U. Manthe, and L. S. Cederbaum, "The multi-configurational time-dependent Hartree approach," *Chemical Physics Letters*, vol. 165, no. 1, pp. 73–78, 1990.

[64] M. H. Beck, A. Jäckle, G. A. Worth, and H. D. Meyer, "The multiconfiguration time-dependent Hartree (MCTDH) method: a highly efficient algorithm for propagating wavepackets," *Physics Report*, vol. 324, no. 1, pp. 1–105, 2000.

[65] G. A. Worth, M. H. Beck, A. Jäckle, and H.-D. Meyer, The MCTDH Package, Version 8.2, 2000, University of Heidelberg, Germany. H.-D. Meyer, Version 8.3, 2002, Version 8.4, 2007, http://mctdh.uni-hd.de.